Engineering natural photosynthesis

Groot, H.J.M. de; Ginley, D.; Cahen, D.

28 Engineering natural photosynthesis

Huub J. M. de Groot
Leiden Institute of Chemistry, Leiden University, Leiden, the Netherlands

28.1 Focus

What is called in this chapter the "engineering" of natural photosynthesis has been performed by evolution over several billions of years. Its optimization, against thermodynamic and other selection criteria from the biological environment, has led to a remarkably limited set of molecular and supramolecular motifs. Photosynthesis starts with absorption of light by mutually interacting chlorophyll (Chl) and related molecules. These are embedded in protein matrices that promote rapid transport of energy by excitons and lower the energy of transition states for charge separation and multielectron catalysis. An understanding of engineered natural photosynthesis is the underpinning of the design of artificial solar-to-fuel devices.

28.2 Synopsis[1]

Light energy is abundant and evenly spread over the surface of the Earth, and virtually all organisms depend on the conversion and chemical storage of light energy by natural photosynthesis. The advent of natural photosynthesis opened up new energy conversion pathways for progression toward thermodynamic equilibrium between the very hot Sun and the much colder Earth. The first-principles thermodynamic and mechanistic analysis of how natural photosynthesis is engineered by biological evolution in this chapter shows that combining different functionalities of light harvesting, charge separation, and catalysis in small molecules or at a single narrow interface is incompatible with high solar-to-fuel conversion efficiency, and that possible solutions to the problem of accumulation of solar energy in chemicals require complex device topologies. This led biology to a modular design approach that is the basis of photosynthesis. It is the result of an intensive evolutionary effort of shaping complex structures, driven by the abundant solar energy spread over the planet.

The molecular basis of photosynthesis is in protein complexes that contain chlorophylls, molecules with good absorbance and a long excited-state lifetime. Photons are captured by light-harvesting antenna complexes, and the energy is rapidly transferred to reaction centers to produce electrical charges of opposite polarity and then an electrochemical membrane potential. Photosynthesis can be divided into the oxygenic (O_2-producing) photosynthesis processes of plants, green algae, and cyanobacteria, and non-oxygenic photosynthesis that occurs in purple bacteria and green sulfur bacteria, for example. Photosynthetic processes separate H^+ and e^- for synthesis of ATP, NAD(P)H and ultimately CO_2 fixation, to produce carbohydrates such as starch and glycogen to store H^+ and e^- in CO_2-neutral fuels. In plants, the photosynthesis machinery is embedded in the thylakoid membrane inside organelles called chloroplasts, whereas in bacteria it is part of the plasma membrane (see Chapter 24).

A modular structure with compartments for light harvesting and charge separation provides flexibility for systems design and adaptation against the natural environmental constraints. Biology uses a small set of active components, most notably interacting chlorophylls to initiate the photochemistry and metal ions for multielectron catalysis, while maintaining the underlying design principles.

[1] Most of the concepts, acronyms, and abbreviations employed are defined within the chapter, but the reader is advised to consult also Chapter 24, in case of doubt.

https://doi.org/10.1017/CBO9780511718786.032 Published online by Cambridge University Press

28.3 Historical perspective

Evolution proceeds by the interaction between diversification at the basis of the biological hierarchy, namely the molecular structure and supramolecular organization, and selection from the top levels, namely the physics, chemistry, and biology of the environment. Driven by the energy they themselves collected from the Sun, the molecular machines of natural photosynthesis have been engineered by evolution to adapt to the biological, hierarchical, order and the environmental settings [1]. However, although photosynthesis occurs in different ways, its basic architectures and operational principles have been largely preserved during the diversification into higher organisms and its basic engineering principles are shared across taxonomic boundaries.

Early photosynthetic species were not able to generate the high redox potential to oxidize H_2O and used H_2, H_2S, and other anaerobic electron donors as sources of electrons. The first photosynthesizers that extract electrons from water have been found, by micropaleontologists, in stromatolites, bacterial fossils, which show that oxygen-evolving cyanobacteria appeared around 2.6 billion years ago, and these started to oxygenate the atmosphere around 2.4 billion years ago (Figure 28.1). About a billion years ago, eukaryotic organisms started symbiotic relationships with these cyanobacteria. The chloroplasts in modern plants are the descendants of these ancient endosymbiotic events [2]. They excrete simple sugars such as glucose and produce the raw construction materials from which plants manufacture many other substances such as complex carbohydrates like starch, lipids, proteins, and lignocellulose.

In recent years structural biology, biophysics, and molecular phylogenetics have provided insight into the modular structure, the operational mechanisms, and the evolution of the molecular machinery of the photosynthetic apparatus. Photosynthesis uses antennae compartments for light harvesting and reaction-center complexes for charge separation. The oxygenic photosynthesis in higher organisms requires two light reactions and two photosystems, photosystem I (PSI) and photosystem II (PSII) [3]. The PSII water-oxidation catalysis can proceed on the millisecond time scale in high light for up to half an hour before the complex is irreversibly damaged, which means that the natural complex can oxidize water at high efficiency for hundreds of thousands of cycles. In contrast, the anoxygenic bacteria at the early stages of the evolution of photosynthesis have only one photosystem, either the type 1 found in green bacteria that is similar to PSI, or the type 2 found in purple bacteria that is similar to PSII (Figure 28.2) [4]. Evidence is currently converging to indicate that oxygenic photosynthesis evolved from lateral gene transfer across species that produced the two important symbiotic fusion events in the evolutionary history of engineered natural photosynthesis: the formation of a cyanobacterium and the development of the chloroplast [1].

28.4 Discussion

In plants and green algae, the photochemical conversion network is in the thylakoid membrane and its biochemical environment. The photosynthetic conversion begins with the harvesting of light, and proceeds via

Figure 28.1. Stromatolites are the oldest fossils, of cyanobacteria that started to emerge several billion years ago and oxygenated the atmosphere. From Wikipedia commons, http://commons.wikimedia.org/wiki/File:Stromatolites_in_Shark_Bay.jp.

https://doi.org/10.1017/CBO9780511718786.032 Published online by Cambridge University Press

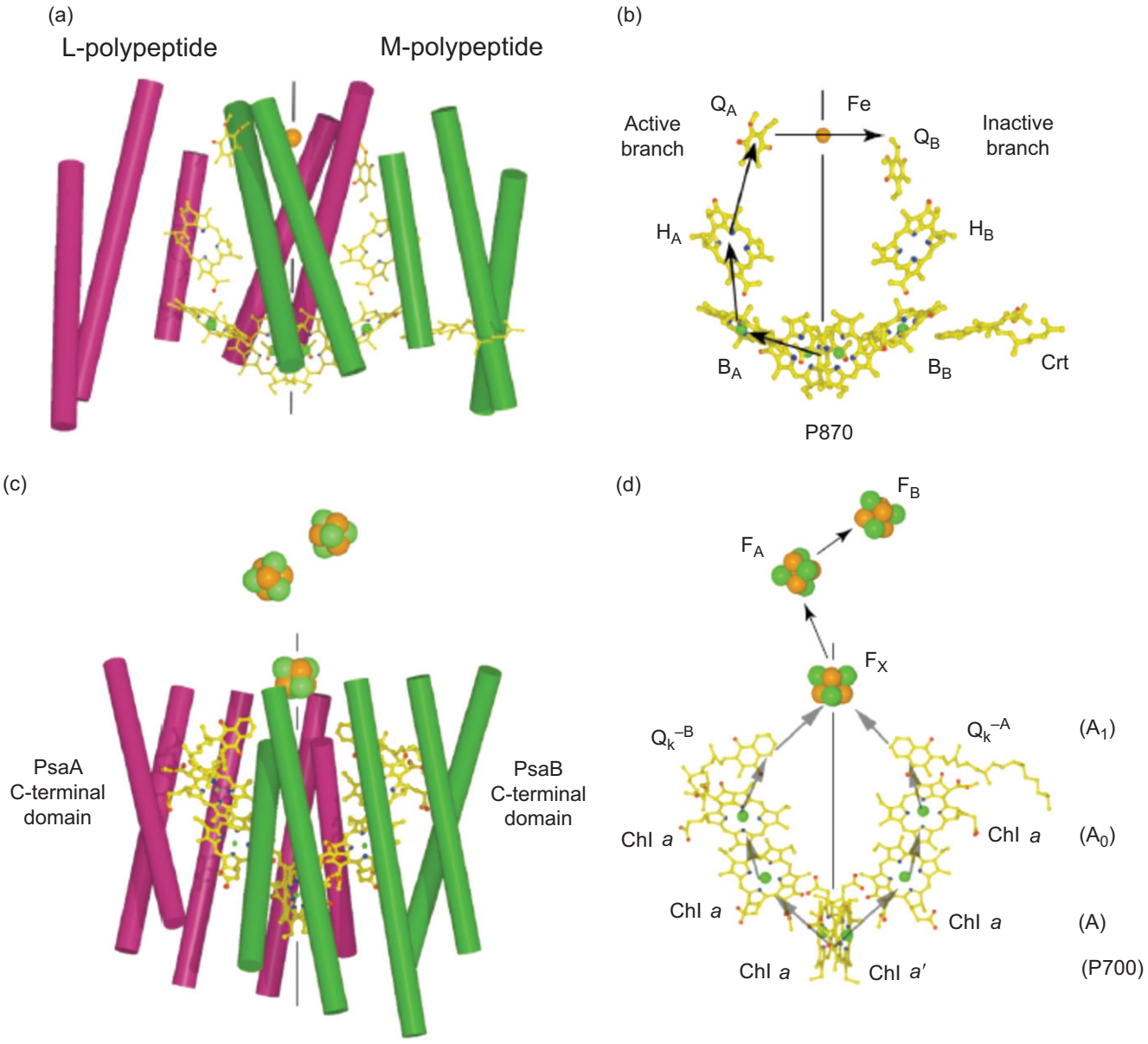

Figure 28.2. The transmembrane helix homology and scaffolding of the cofactors in type-2, (a) and (b), and type-1, (c) and (d), reaction centers. From [1].

trans-membrane charge separation, photochemical oxidation of water, and electron and proton transport, to the Calvin–Benson cycle whereby carbohydrates are synthesized from dilute atmospheric CO_2. The two photosystems, PSII and PSI, operate in tandem, and incoming photons generate the excited states PSII* and PSI*. Both act as strong reducing agents, and leave the reaction-center chlorophyll in an oxidized form. The PSII chlorophyll oxidizes the tetramanganese O_2-evolving complex that accumulates positive charge by extracting electrons from water,

$$2H_2O \longrightarrow O_2 + 4H^+ + 4e^-,$$

and produces O_2. The Z-scheme of photosynthesis in Figure 28.3 indicates how the electrons pass through a redox gradient over the pheophytin (Pheo) and quinones (Q_A and Q_B) to the cytochrome b_6f complex (the box in the diagram) and on to the photo-oxidized PSI [5]. The electron from PSI passes through quinones (A_0 and A_1) and iron–sulfur clusters ($FeS_{x,A\&B}$) to reach ferredoxin (Fd) that reduces $NADP^+$. In an alternative pathway, the electrons from ferredoxin are transferred back to the plastocyanin (Pc) electron-transfer protein via the cytochrome b_6f complex. This cyclic electron transport, which does not require the input of free energy by PSII, results in a trans-membrane electrochemical gradient

https://doi.org/10.1017/CBO9780511718786.032 Published online by Cambridge University Press

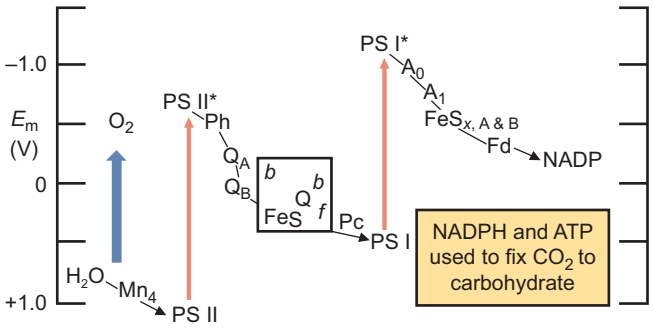

Figure 28.3. The Z-scheme and midpoint electrochemical potentials E_m of electron transfer in oxygenic photosynthesis in plants. Adapted From [5].

that can be used to produce ATP. NADPH and ATP are used to reduce CO_2 to carbohydrates in the subsequent dark reactions of the Calvin–Benson cycle. Thus, with a second photochemical step coupled to the dark reactions

$$CO_2 + 4H^+ + 4e^- \longrightarrow H_2CO + H_2O,$$

the electrons and protons are fed into the metabolic network of the organism, and are utilized for the synthesis of ATP and for the Calvin–Benson cycle that chemically balances the production of energy with the energy demand from the organism with a carbohydrate "fuel" reserve.

Each of the two half-reactions requires four photons, and together they lead to the net production of carbohydrate fuel via transported protons and electrons, using ATP and NADPH as intermediate energy carriers. To reduce one molecule of CO_2 requires a minimum of eight quanta of light. However, if the additional energy needs for cell maintenance and for concentrating CO_2 are also considered, 10–12 quanta are required.

The principal molecular design of the helix and cofactor arrangement of photosynthetic reaction centers is highly conserved in evolution and is used both by micro-organisms and by the chloroplasts of plants and algae [6]. The trans-membrane helix homology and the similarities in the positioning of the cofactors between type-2 and type-1 reaction centers reveal a common origin in the biological evolution (Figure 28.2). The left panels of Figure 28.2 show the trans-membrane helix homology between a type-2 bacterial reaction center, RC, in (a), and PSI, in (c); and the right panels illustrate the homology in the cofactor arrangement: both type-1 and type-2 reaction centers contain six chlorophyll-type rings and two quinone-type molecules. The arrows indicate the directions of the electron transfers. Photosystem I contains three Fe–S clusters. In contrast to the bacterial type-2 RC, PSII has in addition the Mn_4Ca O_2-evolving complex that catalyzes the water-oxidation reaction.

The PSI core is a type-1 reaction center consisting of 11–13 protein subunits. An X-ray structure of PSI has been obtained at 2.5-Å resolution [7]. The two largest subunits, PsaA and PsaB, comprise a heterodimer that binds the majority of the reaction-center cofactors and core antenna pigments. Photosystem I contains an integral antenna system consisting of about 90 Chl *a* molecules and 22 carotenoids. The antenna pigments can be divided into three regions. Some antenna pigments surround the inner core, and there are two peripheral regions where chlorophylls form layers on the stromal and luminal sides of the membrane. Excitation of the antenna pigments results in a rapid equilibrium distribution of the energy among the antenna chlorophylls with a lifetime of 4–8 ps [7]. The rate of energy transfer from the antenna system to P700 RC varies between 20 and 35 ps^{-1} and depends on the organism and the antenna size.

The PSII core complex consists of 19 proteins (Figure 28.4) [4]. There is a type-2 RC complex inside, which contains four Chl *a* molecules that are coupled to form the P680 oligomer. In addition, there are two pheophytin *a* molecules and two plastoquinones in a heterodimeric protein scaffold, formed by two subunits, denoted D1 and D2, that match the L and M helix and cofactor arrangement of the bacterial reaction center in the upper panels of Figure 28.2 [8]. Excitons, formed in the light-harvesting stage, become delocalized over the P680 chlorophylls within 100–500 fs. An intermediate charge-transfer state $Chl^{+\bullet}Pheo^{-\bullet}$ is formed between a chlorophyll donor and a pheophytin acceptor on a time scale of 1.5 ps [9]. Electron transfer proceeds further to the first plastoquinone Q_A within 200 ps; $Q_A^{-\bullet}$, then doubly reduces the secondary quinone acceptor, Q_B, with the possible involvement of a non-heme Fe, located on the pseudo-C_2 axis, with time constants of 0.2–0.4 ms and 0.6–0.8 ms for the first and second reductions, respectively. After receiving two protons, Q_B then leaves its binding pocket as a plastoquinol molecule. The plastoquinol then diffuses out of the protein to be oxidized by cytochrome b_6f (Figure 28.3).

Purple non-sulfur bacteria contain a very-well-studied photosynthetic apparatus, which consists of two light-harvesting (LH) pigment–protein complexes (LH1 and LH2) and a type-2 reaction center [10]. The pigment–protein complexes are membrane-bound and utilize bacteriochlorins and carotenoids for light harvesting [11]. Green sulfur bacteria use large aggregates of up to 100,000 bacterochlorophyll *c*, *d*, or *e* molecules that are contained in vesicles called chlorosomes [12]. The energy harvested by these chlorosomes is transferred via a Fenna–Matthews–Olson antenna protein complex to the membrane-bound reaction center [13]. Cyanobacteria use large peripheral phycobilisomes as their major light-harvesting system. The phycobilisomes

https://doi.org/10.1017/CBO9780511718786.032 Published online by Cambridge University Press

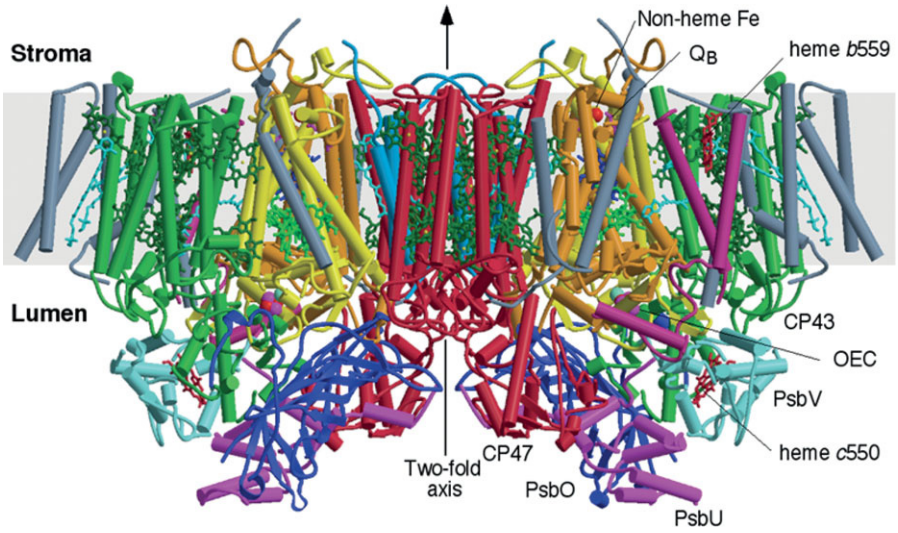

Figure 28.4. The architecture of the photosystem II water-splitting enzyme complex from *Thermosynechococcus elongatus* determined by X-ray crystallography. From [8].

funnel absorbed energy down into the membrane and supply excitation energy to PSI and PSII [14].

The solar energy that is harvested and converted sustains the biological steady state of a photosynthetic organism, and the stability that arises from this homeostasis allows a photosynthetic species to probe and alter its genome and transcriptome for evolution. In this way mutation and development work to engineer natural photosynthesis for a particular environment. Photosynthetic organisms partition their resources between electron transport and metabolism, so that these component processes co-limit photosynthesis. While the photosynthetic reaction centers are highly conserved across species, other parts of the photosynthetic apparatus, such as the antenna (LH) system, are not. The composition of the photosynthetic apparatus is affected by adaptation to the light environment or the chemical environment, such as Fe availability for marine organisms. Changes can occur at the level of the concentration and interaction of participating molecules, the dynamic functional structure of the thylakoid membrane, the number of cells, the leaf architecture, and the way the plants and other photosynthetic organisms are designed and store the harvested energy in a sink or reservoir.

28.4.1 The thermodynamics of photosynthesis is a matter of buying time

To understand how thermodynamic principles constrain engineered natural photosynthesis, it is instructive to look briefly at photovoltaic (PV) conversion by solar cells (cf. Chapters 18 and 19). In a silicon solar cell, photons are harvested by transfer of electrons from the valence band into the conduction band. In a short time the electrons are thermalized to the 1.1-eV bandgap energy, the energy that will determine what can be measured as the open voltage of a solar cell when it is not producing current [15]. The excited electrons in the conduction band of the silicon can decay to the ground state by emission of a photon, unless there is a piece of equipment connected to the solar cell that takes the electrons out of the conduction band and uses the energy (cf. Chapter 18).

Four loss mechanisms limit the maximum power efficiency of a solar cell under non-concentrated blackbody solar radiation to ~31%, the Shockley–Queisser or detailed-balance limit [15]. First, photons with energy below the bandgap energy are not absorbed. Second, thermalization of electrons excited by photons with energy greater than the band gap leads to energy losses by vibrational cooling. Third, the maximum free-energy storage resulting from light absorption is always less than the bandgap energy. Fourth, radiative-recombination losses occur at the absorber due to partial thermodynamic reversibility [16].

Natural photosynthesis uses molecular absorbers and thus is subject to the Shockley–Queisser limit. They convert solar energy in the wavelength region between 400 and 700 nm for storage into chemicals. Photosynthetic energy conversion is engineered to favor the forward reaction for chemical storage of energy against the back reaction and recombination losses in the chlorophyll by fluorescence [17]. For power conversion into chemical storage, photoexcited electrons have to be extracted rapidly from the chlorophyll absorbers. To achieve this, natural photosystems optimize photosynthetic performance with specific arrangements of cofactors and protein modules. The understanding of how this works leads to design principles, fundamental ideas that can serve to guide the design of artificial photosynthesis mimics. One principal element is modularity, the

https://doi.org/10.1017/CBO9780511718786.032 Published online by Cambridge University Press

concept that photosystems and conversion pathways are composed of modules, protein–cofactor matrices that self-assemble into three-dimensional biological structures. They change their physical and chemical properties in a dynamic response mechanism that is encoded by the self-assembly of the polypeptides and cofactors to overcome the barriers to energy transfer, charge separation, and multielectron catalysis.

In photosynthesis, nearly always chlorophyll molecules are the most abundant photon absorbers. Upon excitation, a localized electron–hole pair is created by moving an electron from the highest occupied molecular orbital (HOMO) to the lowest unoccupied molecular orbital (LUMO) in a molecule or in an oligomer of strongly interacting molecules P, to form the excited state P^*. The HOMO–LUMO energy difference $h\nu_0$ plays the role of a semiconductor bandgap. The chlorophyll *a* in plants operates with a HOMO–LUMO gap of $h\nu_0 =$ 1.8 eV, while the bacteriochlorophylls in photosynthetic micro-organisms have $h\nu_0 = 1.4$ eV, and this will be the internal energy of the electrons after thermalization by vibrational cooling.

In its ground state P the molecules are at a chemical potential

$$\mu = \mu_0 + k_B T \ \ln \ p, \tag{28.1}$$

with the chemical potential of P^* given by

$$\mu^* = \mu_0^* + k_B T \ \ln \ p^*. \tag{28.2}$$

These chemical potentials are defined on a molecular scale in electron volts (eV). Here μ_0 represents the energy of P and μ_0^* the energy of P^*, while p and p^* are the molecular fractions of P and P^*, respectively, which are proportional to the concentration of each species in the bulk [18]. The difference in chemical potential between P* and P is $\Delta\mu_{abs} = \mu^* - \mu$. In the absorber $\mu_0^* - \mu_0 = h\nu_0$, the HOMO–LUMO gap. This leads to

$$\Delta\mu_{abs} = h\nu_0 + k_B T \ \ln\left(\frac{p^*}{p}\right). \tag{28.3}$$

Here the second term represents the entropy of mixing, which is due to the mixing of the ground state and the excited state in the same molecular volume [17]. In the dark the excited and ground state are in thermodynamic equilibrium and $\Delta\mu_{abs} = 0$, leading to $p^*/p = \exp[-h\nu_0/(k_B T)]$, the Boltzmann distribution [18].

When exposed to sunlight, the absorber is excited at a rate g by solar photons, while the excited state is quenched via fluorescence at a decay rate τ^{-1} according to

$$P \underset{1/\tau}{\overset{g}{\rightleftarrows}} P^*.$$

These processes will shift the population distribution, according to $p^*/p = g\tau$; another activation/deactivation equilibrium is then established, with $\Delta\mu_{abs} \neq 0$, and thus free energy can be extracted from the chlorophyll donor absorber [18].

Since the chlorophyll excited state decays to the ground state by the fluorescence in τ in a short time, on the order of nanoseconds for chlorophylls in proteins, the type-1 and type-2 RCs need to transfer excited electrons in a shorter time from P^*, into an excited-state acceptor sink Q to produce an electron–hole pair,

$$P \underset{1/\tau}{\overset{g}{\rightleftarrows}} P^* \underset{I_b}{\overset{I_f}{\rightleftarrows}} P^+Q^-,$$

with the electron on Q and the hole on P. In the dark, the molecular fraction of electron–hole pairs is $p_h q_e$, with

$$\mu_{pair} = \mu_{0,pair} + k_B T \ \ln(p_h q_e) \tag{28.4}$$

for the chemical potential for the donor–acceptor pair. For the excited pair

$$\mu^*_{pair} = \mu^*_{0,pair} + k_B T \ \ln(p^*_h q^*_e), \tag{28.5}$$

with $p^*_h q^*_e$ the concentration of electron–hole pairs after absorption of a photon [18]. The physical limit for energy storage by the pair is

$$\Delta\mu_{st} = h\nu_0 + k_B T \ \ln\left(\frac{p^*_h q^*_e}{p_h q_e}\right). \tag{28.6}$$

Here the entropic term measures the concentration of electron–hole pairs in the charge-separated state, i.e., the probabilities of electron and hole occupation of the acceptor and donor states, in the light relative to the concentration in the dark.

Upon excitation with light, a charge-separated state is produced at a forward transfer rate I_f, in steady-state equilibrium with the backward transfer rate I_b, and

$$\frac{p^*_h q^*_e}{p_h q_e} = \frac{I_f}{I_b}. \tag{28.7}$$

The backward rate is the inverse of the lifetime of the storage reservoir $I_b = t^{-1}$, while the forward rate is constrained by the fluorescence lifetime of the absorber $I_f = \tau^{-1}$. This leads to a time-dependent limit for photochemical storage of energy

$$\Delta\mu_{st} = h\nu_0 - k_B T \ \ln\left(\frac{t}{\tau}\right). \tag{28.8}$$

The longer the energy needs to be stored, the more entropy of mixing needs to be generated in the chemical network for storage in order to prevent loss of energy due to fluorescence at the start of the conversion chain in competition with the storage [19]. Equation (28.8) is the consequence of time-reversal symmetry, and is rooted deeply in the first principles of the physical world. (Hamiltonians are Hermitian and time development operators in quantum theory are therefore unitary.

https://doi.org/10.1017/CBO9780511718786.032 Published online by Cambridge University Press

This leads to time-reversal symmetry and the second law of thermodynamics.)

In oxygenic photosynthesis, the fluorescence lifetime is also very short, compared with the required storage times for water-oxidation catalysis, which is the most difficult reaction in natural photosynthesis. Water oxidation is a four-electron reaction that is rate-limited at a time scale of milliseconds, and, according to Equation (28.8) the storage of electrons on this time scale requires a mixing entropy of at least ~0.6 eV [20]. This is a significant part of the incoming $h\nu_0 = 1.8$ eV for the chlorophyll *a* absorber. The four positive charges have to be accumulated in a small catalytic site to split the water and form the O—O bond on the Ångström scale, which is very small compared with the wavelength of optical absorption of 700 nm. To achieve this, natural photosynthetic systems are engineered to harvest the photons in antenna systems, separate charges in reaction centers by efficient quantum delocalization and electron tunneling in a redox gradient, and concentrate charges into a catalytic site by a proper match of time scales and length scales in dedicated photosynthetic membrane topologies [21]. From Equation (28.8) it follows that, for the desired storage times to balance production and demand in human energy use, in the range of days to years, around 50% of the energy after thermalization cannot be extracted [20]. This is a principal difference between PV and photochemistry, insofar as PV-produced electricity can be transported rapidly to locations where energy is required, which eliminates the need for storage and the accompanying losses. On the other hand, natural photosynthesis at its best is remarkably efficiently engineered. Calculations project conversion efficiency as high as 9% for prokaryotic micro-organisms which includes thermalization and long-term storage (cf. Chapter 24) [22].

28.4.2 Engineered light-harvesting modules

Natural light-harvesting antennae permit an organism to increase greatly the absorption cross section for light and transport of energy on a very short time scale. The intensity of sunlight is dilute, and every single pigment molecule absorbs at most a few photons per second. To sustain the catalysis for photosynthesis at the limiting rate of 10^{-3}–10^{-4} s, several hundred pigments are incorporated into supramolecular assemblies of antenna units. They cover large photosynthetic membrane surfaces to ensure that photons striking any spot on the surface will be absorbed and concentrated for feeding energy quanta into the reaction center where charge separation and electron transport take place. An example of a photosynthetic membrane topology is shown in Figure 28.5(a), for bacterial photosynthesis, which is based on three membrane protein complexes, two light-harvesting antennae, denoted LHI and LHII, and a reaction-center complex RC [11]. The antenna units transfer the energy from light by exciton migration over long distances to the RCs. They surround the RCs, optimizing the energy-transfer efficiency by use of multiple antenna–RC connections [23].

The LHII antenna, which is the most abundant one, contains two chlorophyll species, B800 with maximum absorption at $\lambda_{max} = 800$ nm and B850 with $\lambda_{max} = 850$ nm. In the ground state the LHII antennae are highly ordered, almost-crystalline assemblies of trans-membrane polypeptides with many pigment-binding sites. They increase the absorption cross section by containing densely packed dye molecules with inhomogeneously broadened optical absorption profiles. Chlorophylls are moderately sized molecules that are sterically crowded in the side chains to the central chlorin macro-aromatic cycle. This makes for an almost flat energy landscape of the macro-aromatic cycle, and the distortion of the chlorin ring is primarily along only the six lowest-frequency normal coordinates [24]. The optical broadening in an otherwise extremely homogeneous structure can be enhanced by induced misfits, namely local spots of structural frustration that are established in the folding and self-assembly process of the complex [25][26]. The structural frustration leads to an energy landscape that favors thermally activated modulation of the energy levels among the chlorophylls within a single antenna or reaction center complex on time scales that are long compared with those of the energy-absorption and charge-transfer processes and produces inhomogeneous broadening of the electronic transitions due to ensemble averaging [27]. For B850 there is considerable physical frustration in the histidine ligands to the central Mg^{2+} ion of the B850 chlorophylls. These histidines are hydrogen bonded to the protein, and stabilize the ring V keto functionality of a neighboring chlorophyll in an anti-parallel orientation. They exhibit an anomalous electronic hybridization and stabilize positive charge due to stress and strain exerted by the protein complex [28].

The chlorophylls in the B800 and B850 rings strongly overlap, and, when they absorb light, collective electronic excitations that are promoted by quantum delocalization over the electronically coupled pigments are formed [29]. However, the exciton–phonon coupling leads to classical confinement by structural reorganization of the pigments and to symmetry breaking by a polaronic contribution to the excitons that is of chlorophyll–chlorophyll charge-transfer character, while the modulation of the electronic transition energies by slow conformational changes produces electronic disorder. Both lead to more localized exciton wavefunctions that extend over four to six chlorophylls in the rings [27]. The excitation dynamics in the antennae is a superposition of coherent motion of delocalized

https://doi.org/10.1017/CBO9780511718786.032 Published online by Cambridge University Press

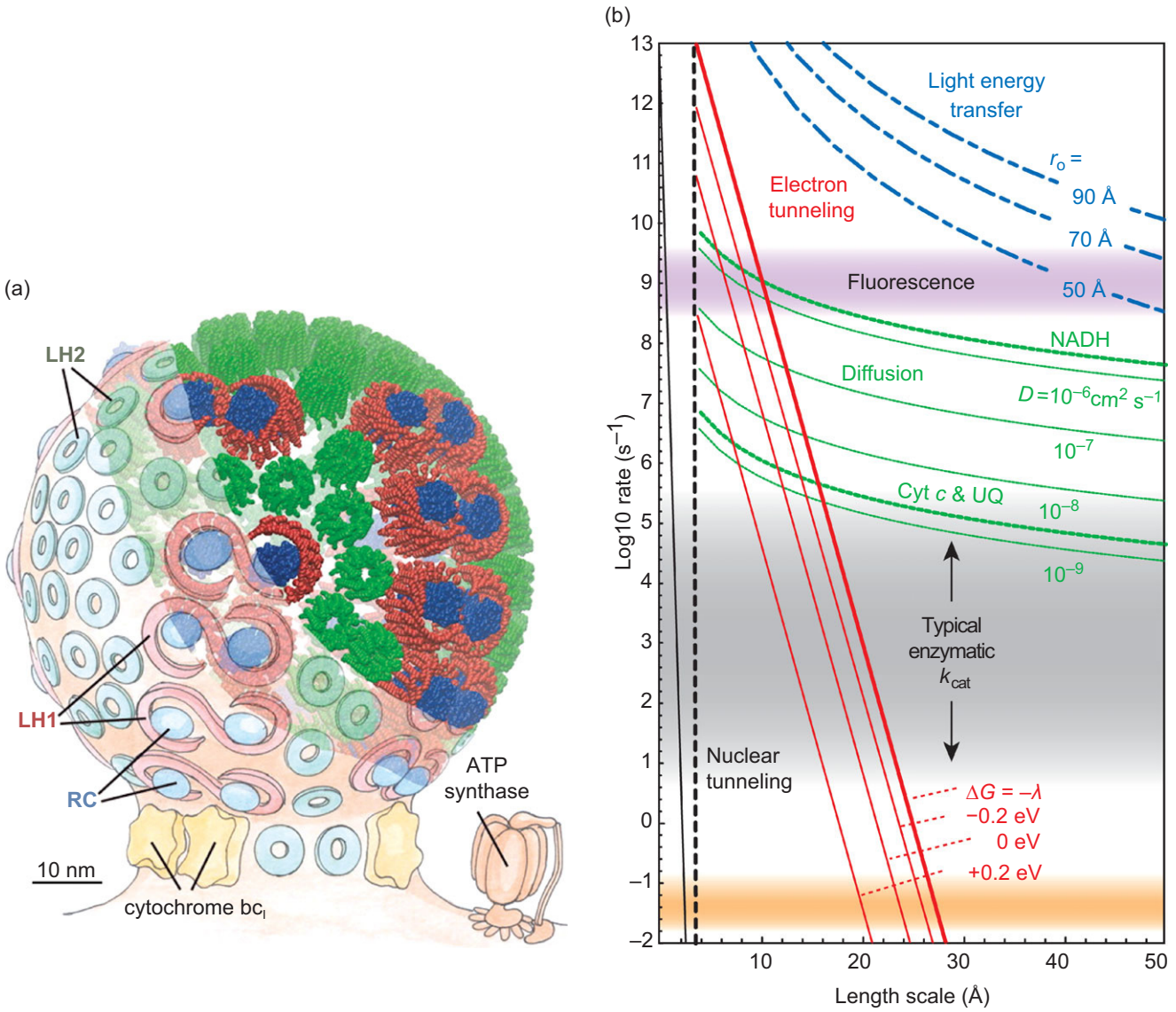

Figure 28.5. (a) A model of the photosynthetic unit of purple bacteria showing the arrangement of light harvesting units 1 and 2 (LHI and LHII) and the reaction center (RC). The structures of LHII and the RC have been determined by X-ray crystallography, and LHI is simulated by analogy to LHII. From [11] (b) Time scales and length scales of energy and electron transfer in photosynthesis. From [21].

excitons on a time scale of 100 fs, hopping on a time scale of 350 ps, and pinning of localized excitations. In single LHII complexes it is possible to observe the switching between these regimes. Apparently the antennae in bacterial photosynthesis are engineered to accommodate mutually interacting chlorophylls that produce a heterogeneous manifold of excited states, including excitons with a high degree of delocalization in combination with more localized excitations due to the presence of weakly coupled pigments. The basic mechanism of photosynthetic light harvesting for the delivery of excitation energy to the reaction centers includes fast relaxation between exciton states on a femtosecond time scale within strongly coupled chlorophyll clusters and slower energy migration on a picosecond time scale between clusters or monomeric sites [27].

The major type of peripheral antennae in green plants, LHCII, is a trimer, with different chlorophyll species that mutually interact and carotenoids that have a strong excitonic coupling with the chlorophyll pigments to achieve efficient energy transfer as accessory light-harvesting pigments by absorbing light energy in the visible spectrum that is unavailable to chlorophylls (Figure 28.6) [30]. As for the bacterial antennae, clusters

https://doi.org/10.1017/CBO9780511718786.032 Published online by Cambridge University Press

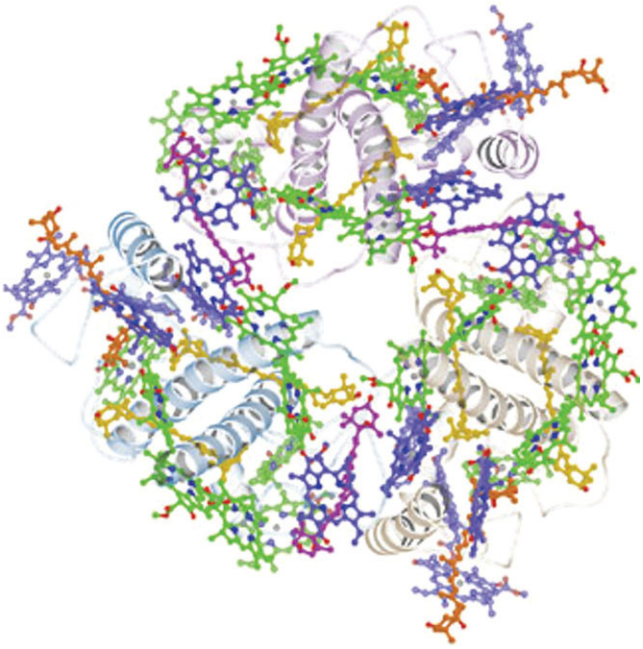

Figure 28.6. The crystal structure of the LHCII antenna trimer from spinach. From [30].

of strongly coupled pigments depopulate on a short time scale by a combination of coherent transfer and hopping into a sink formed by chlorophyll *a* on the outside of the trimer to feed the energy into plant PSI or PSII. Since the performance and survival of plants in natural environments rely on their ability to actively adapt to variable light intensity, an important additional design feature of the LHCII photosynthetic complexes is their built-in mechanism for the dissipation of excess energy [31]. In the shade, light is efficiently harvested in photosynthesis. However, in full sunlight, much of the energy absorbed cannot be processed and photoprotection regulation mechanisms have evolved to protect the conversion chain against photo-oxidative damage. The redox state of the cytochrome b_6f complex induces state transitions, in which the LHCII shuttles between PSI and PSII, balancing the electron transport. In addition, when overproduction of protons by the photosystems leads to acidification of the lumen, the LHCII antenna can rapidly switch to a conformational state that safely dissipates the excess energy as heat by non-photochemical quenching (NPQ) mechanisms involving excited states of chlorophylls or carotenoids [32][33][34]. The deprotonation of a pH-sensing protein, PsbS, controls reversible oligomerization of the LHCII via a chemical conversion of violaxanthin carotenoids to stabilize the LHCII assemblies. This can give rise to symmetry breaking whereby a polaronic contribution to the excitons becomes dominant and leads to the formation of localized chlorophyll–chlorophyll charge-transfer states with an enhanced coupling to the ground state to produce NPQ on a time scale of a few hundred picoseconds [32]. Alternatively, a channel for energy dissipation by transfer to a bound carotenoid can open up [33][34].

To support long-range excitation transfer, groups of tightly coupled pigments are coupled to other groups and RCs by the Förster resonant-transfer (FRET) mechanism with first-order energy-transfer rate

$$k_e = (r_0/r)^6/\tau, \tag{28.9}$$

due to Coulomb dipole–dipole interactions [35]. The migration rate is inversely proportional to the fluorescence lifetime and r_0 is the distance at which the transfer efficiency is 50%. Figure 28.5(b) shows the transfer ranges for $\tau = 10^{-9}$ s and $r_0 = 50$, 70, or 90 Å [21]. For conservation of energy, strong optical overlap between the donor and acceptor complexes is beneficial.

The length scale of exciton migration in the antenna is considerable, and the exciton lifetimes should be long enough to allow photons striking any part of the antenna to reach the RC. Once excitons have been trapped in the RC, the process of charge separation should take place faster than back-transfer to the antenna units. In photosynthetic assemblies this is achieved by having a relatively large antenna–RC distance versus a short distance for the redox pigments in the RC, in a topology such that RCs are surrounded by assemblies of antenna pigments giving a spatial arrangement in which energy transfer is optimized by multiple contact points for the transfer of excitons to the RC (Figure 28.5(a)).

There is an exception, however, in chlorosome antennae that are engineered by biological evolution to operate under environmental conditions where light is a limiting factor. Chlorosomes are anomalous in the sense that they are engineered to sustain extended polarons, where quantum delocalization is combined with symmetry breaking of the lowest exciton state to gain polaronic charge-transfer character while at the same time extending the system across many chlorophylls [36]. Chlorosomes are the largest and fastest light-harvesting antennae found in nature and are constructed from hundreds of thousands of self-assembled bacteriochlorophylls *c*, *d*, or *e*. The pigments are closely packed in stacks, with the stacks aligned to form sheets that self-assemble into coaxial tubes [12]. Following efficient excitation in the direction of the stacks, the biological light-harvesting requirement is fulfilled by providing ultrafast helical exciton-delocalization pathways with polaronic character along helical arrangements of BChl molecules with aligned electric dipoles that are interconnected by polarizable hydrogen bonds (H-bonds) (Figure 28.7) [12][36]. These H-bonds are strained and do not contribute to the stabilization of the aggregate, but transform the helical bacteriochlorophyll array into a material with a high dielectric constant. Consequently,

https://doi.org/10.1017/CBO9780511718786.032 Published online by Cambridge University Press

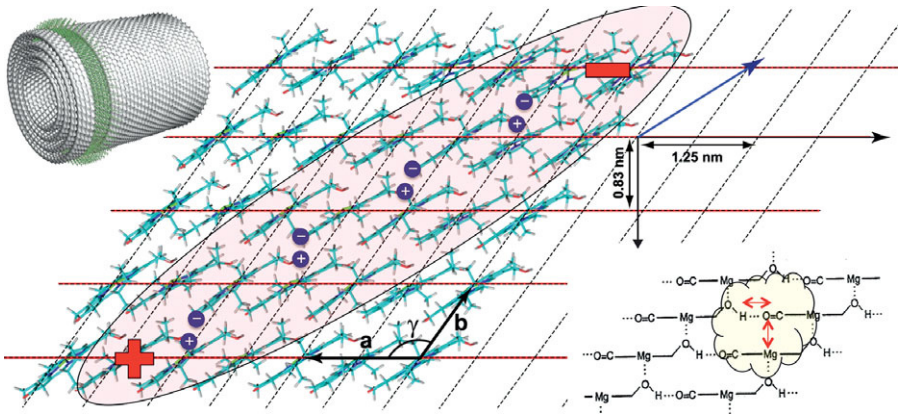

Figure 28.7. The bacteriochlorophylls in chlorosome antenna form stacks and sheets that self-assemble into concentric nanotubes. Upon excitation with light, extended excitons are formed in the direction of the aligned electric dipoles, facilitated by activated hydrogen bonds in the C=O···H—O···Mg motifs in the structure.

electric-field screening tends to reduce the Coulomb interaction between electrons and holes. This favors the symmetry breaking of excitons into extended polarons by the release of mechanical strain in the molecular array of activated hydrogen bonds. This leads to a collinear proton-coupled electron-transfer (PCET)-type mechanism, whereby the symmetry breaking of the exciton is synergistic with the stabilization of the H-bond helix by reorganization of the activated hydrogen bonds. This dielectric response produces a transient shift of the molecular energy levels. The chlorosome is an organelle found in early photosynthesizers and it nicely illustrates how mutually interacting chlorophylls can provide a versatile engineering material, with both energy-transfer and charge-transfer characteristics.

28.4.3 Smart matrices for electron transfer and electrochemistry

Natural photosynthesis achieves a quantum efficiency of 99% under low-light conditions, which is possible only if the forward current rate I_f is faster than the fluorescence decay rate of 10^9 s^{-1} [17]. The quantum efficiency is the ratio of the number of separated e^- and holes to the number of photons in the photosynthetically active region of the spectrum incident on the photosynthetic assembly. In transition-state theory, rates of chemical reactions are described along a potential-energy surface. As reactants gain energy from thermal collisions, they overcome an activation-energy barrier E_a to the transition state, after which they spontaneously decay to the product. The net energy transfer with the surroundings is zero, and the reaction is adiabatic [37]. In solar cells, charge separation is facilitated by an electric field over the depletion region of a p–n junction that separates the light-generated minority and majority carriers. In photosynthetic reaction centers, excitons that enter from the antenna produce excited states P^* that are unstable with respect to symmetry breaking to form first chlorophyll–chlorophyll charge-transfer states and then full charge separation, P^+Q^-, over ~40 Å, the thickness of the biological membrane. The charge separation is mediated by weak electronic overlap between the donor and acceptor and driven by a downhill redox gradient as shown in Figure 28.3 [38]. This is accomplished by placing multiple redox cofactors so that they are separated by an edge-to-edge distance less than 0.6 nm to ensure rapid forward transfer, on a time scale of ~10 ps or less, by downhill dissipative electron tunneling, while increasing the storage time for every step [39]. The electron tunneling rates in weakly coupled donor–acceptor pairs are described well by

$$I_f = \frac{2\pi}{\hbar} V_{PQ} FC, \tag{28.10}$$

with V_{PQ} the electronic matrix coupling element between the donor and the acceptor, and FC a Franck–Condon factor that describes the structural changes that are required in order to overcome the activation barrier in the donor–acceptor pair in the electron-transfer reaction. The structural rearrangements are generally described classically by a harmonic potential to depict how the energy of the precursor complex depends on its nuclear configuration prior to the reaction, while another single-potential surface is used to describe the product complex. This leads to the expression

$$FC = (4\pi\lambda k_B T)^{-1/2} \exp[-E_a/(k_B T)], \tag{28.11}$$

where E_a has a quadratic dependence on the reorganization energy λ and on the standard Gibbs free-energy difference between the products and reactants ΔG° according to

$$E_a = -(\Delta G^\circ - \lambda)^2/(4\lambda). \tag{28.12}$$

For the electron-transfer reaction in proteins the $\Delta G^\circ < 0$ and $\lambda = 0.7$ eV [39]. In the "normal" region the current I_f increases when $-\Delta G^\circ$ increases, until $-\Delta G^\circ = \lambda$, for which there is no barrier to electron-transfer and the electron current reaches a maximum. One of the key features of electron-transfer theory is that it predicts an "inverted region" where the rate of an electron-transfer reaction will slow down when the free energy of the reaction becomes very large, $-\Delta G^\circ > \lambda$ [40].

https://doi.org/10.1017/CBO9780511718786.032 Published online by Cambridge University Press

An analysis of electron-transfer processes in proteins in the classical harmonic approximation reveals a common $\hbar\omega = 70$ meV, which is well above the Boltzmann energy $k_B T = 25$ meV available at room temperature [39]. This is important, since the Marcus theory is derived in the high-temperature limit. Thus, the description given above is self-consistent and subject to refinement. For instance, the electron transfer may be accompanied by proton transfer in a synchronous or asynchronous PCET mechanism [41].

The electron-transfer mechanism is quite insensitive to the thermodynamic driving force, in particular when there is a global match $-\Delta G^\circ \sim \lambda$ [39]. With charge separation over a downhill redox gradient the $\Delta G < 0$, and the electron tunneling current is to a good approximation described by

$$\log I_f = 15 - 0.6r - \frac{3.1(\Delta G + \lambda)^2}{\lambda}. \qquad (28.13)$$

For a specific time $\tau_f = I_f^{-1}$ there is a maximum distance r over which tunneling can proceed, depending on the redox gradient [39]. The fastest transfer rate is obtained for $-\Delta G^\circ = \lambda$, and the red lines in Figure 28.5(b) depict the tunneling behaviour [21]. In the reaction center the tunneling processes serve to bridge the six orders of magnitude between the time scale of fluorescence and the time scale of catalysis (Figure 28.5(b)). At the time scale of catalysis, 10^{-3} s, the tunneling distance is ~20 Å. Thus, a biological membrane of thickness ~40 Å is a good tunneling barrier for the accumulation of charge for catalysis. However, the time scale of fluorescence, 10^{-9} s, requires that efficient charge separation proceeds on a time scale of a few picoseconds. This translates into a tunneling barrier of ~5 Å. Thus, for a high quantum efficiency the distance between P^+ and Q^- needs to be 5 Å, while for the accumulation of charge for catalysis the distance between P^+ and Q^- needs to be in excess of 20 Å. Natural photosynthesis is engineered to solve this dilemma with multiple intermediates and a sequence of transfer steps with increasing edge-to-edge distance between cofactors and increasing storage times to avoid fluorescence losses by quantum delocalization and tunneling from the product states backwards into the reactant.

In oxygenic photosynthesis, oxidation of water proceeds following the accumulation of four positive charges in the oxygen-evolving complex (OEC), an Mn_4Ca cluster attached to the PSII charge-separation chain (Figures 28.4 and 28.8). It provides a structural framework for describing the water-splitting chemistry of PSII and therefore is of major importance for designing artificial catalytic systems for reproducing this chemistry. While the multielectron catalysis is rate-limited at 10^{-3}–10^{-4} s at high light, a large dynamic range with respect to the incoming photon flux implies

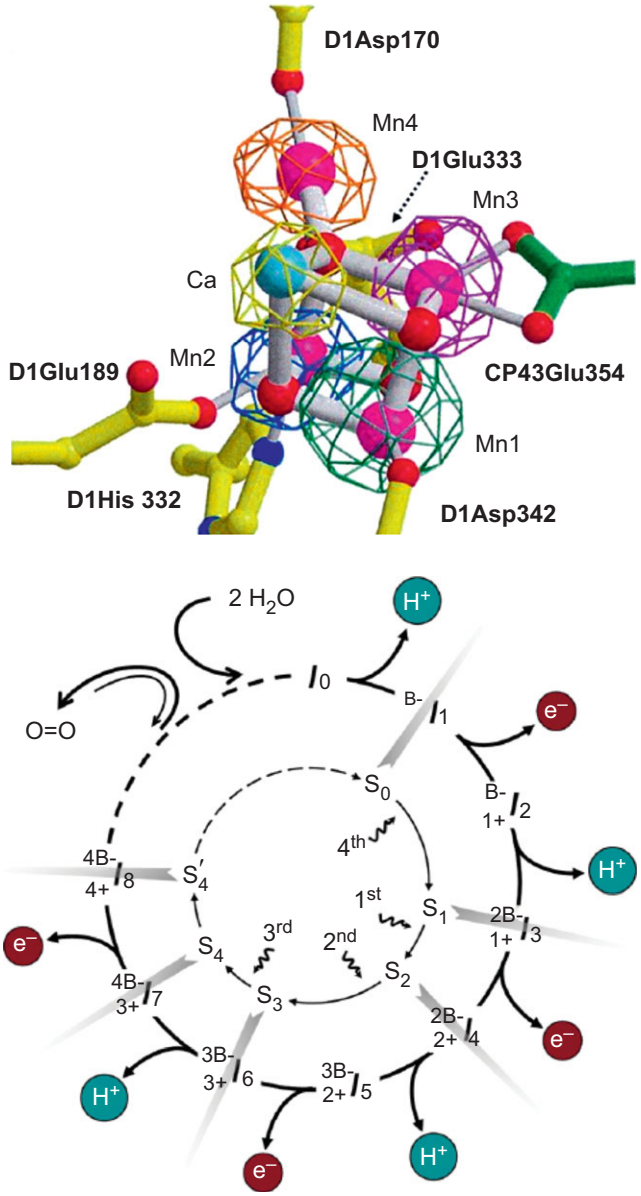

Figure 28.8. The oxygen-evolving complex in *Thermosynechococcus elongatus* [8] and the four-stage proton-coupled electron-transfer catalytic cycle [42].

potentially very long accumulation and storage times of catalytic intermediates in the four-electron water-oxidation cycle when the incoming photon flux is low. Very long accumulation times are possible, provided that the intermediate storage of holes is coupled to the rapid irreversible release of protons from the catalytic site. Here the thermodynamic irreversibility of proton release generates mixing entropy and prevents wasteful back reactions.

The protein environment adjusts the proton chemical potential to the OEC catalytic sites and the resting state of the PSII is the S1 state, with one electron extracted from the OEC, stabilized by proton release (Figure 28.8(b)). To maintain charge neutrality throughout the S-cycle for

https://doi.org/10.1017/CBO9780511718786.032 Published online by Cambridge University Press

leveling of the redox potential, release of electrons into the P680 chlorophylls alternates with the release of H^+ into the protein environment [42][43].

Oxidation of water proceeds with a redox potential difference of at least 1.23 V (vs. NHE). If the catalysis is rate-limited on a time scale of 10^{-3} s, and the oxidation potential needs to be generated with an absorber with a lifetime on the nanosecond scale, the mixing-entropy losses will be equivalent to at least 0.6 eV, as is explained above from the coupling of time scales and energy scales. This leads to a minimal "bandgap" for photon absorption of 1.8 eV. Natural oxygenic photosynthesis employs two reaction centers operating in tandem to compensate for the nonlinear response of the thylakoid membrane assembly and redox gradients associated with downhill electron transport in the catalysts, the cytochrome, and the energy carriers like NADPH [43]. This leads to the Z-scheme for photosynthesis depicted in Figure 28.3.

According to Equation (28.8) the energy difference between the absorber and the OEC is constrained by $h\nu_0 - \Delta\mu_{st} = k_B T \ln(t/\tau)$, and the mixing entropy represents an unavoidable overpotential in the operation of the multielectron catalyst in natural photosynthesis [19]. While the stabilization of intermediates in the charge accumulation can be very long due to irreversible proton release, the overpotential from the mixing entropy can be put to use for the confinement of holes on the time scale of the rate-limiting step in the oxygen-evolution process.

28.5 Summary

The large temperature difference between the Sun and the Earth provides a powerful engine for work on the evolution of the biological steady state and is the only source of sufficient energy for engineering the biodiversity on the planet. The principal molecular design of the helix and cofactor arrangement of photosynthetic reaction centers is highly conserved in evolution and is used both by micro-organisms and by the chloroplasts of plants and algae.

Chemical storage of solar energy requires "buying time" by taking away electrons rapidly at the expense of mixing entropy in the chemical conversion, to prevent the loss of harvested energy by radiative recombination of electron–hole pairs.

Since electrons and holes are very light particles with high tunneling probabilities, natural photosynthetic reaction centers are engineered for charge confinement by phonon dressing in the antenna for energy transfer by neutral excitons, while in the RCs large tunneling barriers prevent leakage from storage sinks back into the absorber and fluorescence losses on the time scales of catalysis.

Light harvesting by chlorosomes exploits the spatial anisotropy in the materials properties of extended chlorophyll aggregates. They combine photon absorption into symmetric excitons along the stacking direction with symmetry breaking into polaronic excitons along the H-bond helix. The latter can extend over tens of monomers for barrierless ultrafast energy transport in less than 200 fs to the RC complex.

Photosynthetic donor–acceptor–protein complexes are "smart matrices" that have been engineered by evolution to stabilize the transition state. Upon excitation with light, strain is released in the form of classically coherent (nuclear) motion with $\hbar\omega = 70$ meV to reorganize the donor–acceptor pair along a trajectory that leads to the matching of the high $\lambda = 0.7$ eV.

In the modular design of engineered natural photosynthesis the tunneling bridge provided by the RC and tuning of the proton chemical potentials for proton-coupled electron transfer at the OEC allow the efficient integration of storage with catalysis for oxidation of water. In particular, the incorporation of an insulating tunneling bridge between the OEC and the electron donor P680 is a critical element in the modular design, since it ensures that the mixing entropy for photoelectrochemical catalysis is utilized to produce an overpotential for the confinement of charge in the OEC catalytic site on the time scale of catalysis.

The information on how photosynthetic organisms are able to use solar energy to extract electrons from water to produce hydrogen or reduced carbon compounds presented in this chapter can be used to design modular photocatalytic systems capable of using solar energy to produce fuels directly from sunlight using water as a raw material (see also Chapter 47). Many scientists are convinced that, by using state-of-the-art knowledge from photosynthesis, the value of current technology for conversion of solar energy into electricity can be raised by adding a storage function, as in natural photosynthetic assemblies, leading to the development of novel robust photoelectrochemical solar fuel producers (see Chapter 49), or "artificial leaves (Chapter 27)."

28.6 Questions for discussion

1. Use Equation (28.8) to estimate the maximum storage time of solar energy by photochemical conversion. Is this longer or shorter than the lifetime of the solar system?
2. The transfer efficiency of the Förster hopping process is $E = k_e/(\tau^{-1} + k_e)$. What is the maximum distance r in units of r_0 for 95%, 90%, and 50% efficiency?
3. Using Equation (28.13) for the long-distance electron transfer in proteins, calculate how many cofactors are needed to span a 40-Å tunneling barrier in 100 μs.

https://doi.org/10.1017/CBO9780511718786.032 Published online by Cambridge University Press

4. If you had a fast water-oxidation catalyst that operates on the microsecond time scale, what would be the thickness of the tunneling barrier for charge confinement in the catalyst? How many cofactors would be needed to bring the electrons to the catalyst when they come from a molecular absorber with a lifetime of 10^{-8}s?
5. Write an essay on how engineered natural photosynthesis inspires the design of artifical solar-to-fuel conversion.

28.7 Further reading

- http://en.wikipedia.org/wiki/Photosynthesis. A short introduction to the biological design and diversity of photosynthesis for the novice reader that is complementary to the materials-engineering perspective of this chapter.
- **R. E. Blankenship**, 2002, *Molecular Mechanisms of Photosynthesis*, Oxford, Blackwell Science. For a comprehensive and in-depth overview of the principles of photosynthesis on an advanced level, this book is an excellent starting point.
- **P. Fromme**, 2008, *Photosynthetic Protein Complexes: A Structural Approach*, Weinheim, Wiley-VCH. This book provides a heuristic overview of how the structures relate to mechanisms of function on the level of the molecular machines involved in the processes of photosynthesis.
- **A. Pandit**, **H. J. M. de Groot**, and **A. Holzwarth**, 2006, *Harnessing Solar Energy for the Production of Clean Fuels*, Strasbourg, (European Science Foundation, http://www.esf.org/publications/lesc.html). This text, on which the present chapter is partly based, provides additional information on how engineered natural photosynthesis inspires the production of clean fuels.

28.8 References

[1] **G. Giacometti** and **G. M. Giacometti**, 2010, "Evolution of photosynthesis and respiration: which came first?," *Appl. Magn. Reson.*, **37**(1), 13–25.

[2] **P. G. Falkowski** and **A. H. Knoll** (eds.), 2007, *Evolution of Primary Producers in the Sea*, San Diego, CA, Academic Press.

[3] **L. N. M. Duysens**, **J. Amesz**, and **B. M. Kamp**, 1961, "Two photochemical systems in photosynthesis," *Nature*, **190**, 510–151.

[4] **I. Grotjohann**, **C. Jolley**, and **P. Fromme**, 2004, "Evolution of photosynthesis and oxygen evolution: implications from the structural comparison of Photosystems I and II,". *Phys. Chem. Chem. Phys.*, **6**(20), 4743–4753.

[5] **R. C. Prince** and **H. S. Kheshgi**, 2005, "The photobiological production of hydrogen: potential efficiency and effectiveness as a renewable fuel," *Crit. Rev. Microbiol.*, **31**, 19–31.

[6] **R. E. Blankenship**, 2002, *Molecular Mechanisms of Photosynthesis*, Oxford, Blackwell Science.

[7] **P. Fromme**, **P. Jordan**, and **N. Krauss**, 2001, "Structure of photosystem I," *Biochim. Biophys. Acta – Bioenergetics*, **1507**(1–3), 5–31.

[8] **K. N. Ferreira**, **T. M. Iverson**, **K. Maghlaoui**, **J. Barber**, and **S. Iwata**, 2004, "Architecture of the photosynthetic oxygen-evolving center," *Science*, **303**(5665), 1831–1838.

[9] **L. M. Yoder**, **A. G. Cole**, and **R. J. Sension**, 2002, "Structure and function in the isolated reaction center complex of photosystem II: energy and charge transfer dynamics and mechanism," *Photosynthesis Res.*, **72**(2), 147–158.

[10] **C. N. Hunter**, 2009, *The Purple Phototrophic Bacteria*, Dordrecht, Springer.

[11] **M. K. Sener**, **J. D. Olsen**, **C. N. Hunter**, and **K. Schulten**, 2007, "Atomic-level structural and functional model of a bacterial photosynthetic membrane vesicle," *Proc. Natl. Acad. Sci.*, **104**(40), 15723–15728.

[12] **S. Ganapathy**, **G. T. Oostergetel**, **P. K. Wawrzyniak**, *et al.*, 2009, "Alternating syn–anti bacteriochlorophylls form concentric helical nanotubes in chlorosomes," *Proc. Natl. Acad. Sci.*, **106**(21), 8525–8530.

[13] **Y. F. Li**, **W. L. Zhou**, **R. E. Blankenship**, and **J. P. Allen**, 1997, "Crystal structure of the bacteriochlorophyll *a* protein from *Chlorobium tepidum*," *J. Mol. Biol.*, **271**(3), 456–471.

[14] **R. MacColl**, 1998, "Cyanobacterial phycobilisomes," *J. Struct. Biol.*, **124**(2–3), 311–334.

[15] **W. Shockley** and **H. J. Queisser**, 1961, "Detailed balance limit of efficiency of p–n junction solar cells," *J. Appl. Phys.*, **32** 510–519.

[16] **M. C. Hanna** and **A. J. Nozik**, 2006, "Solar conversion efficiency of photovoltaic and photoelectrolysis cells with carrier multiplication absorbers," *J. Appl. Phys.*, **100**(7), 074510.

[17] **R. T. Ross** and **M. Calvin**, 1967, "Thermodynamics of light emission and free-energy storage in photosynthesis," *Biophys. J.*, **7**(5), 595–614.

[18] **T. Markvart** and **P. Landsberg**, 2002, "Thermodynamics and reciprocity of solar energy conversion," *Physica E*, **14**(1–2), 71–7.

[19] **H. J. M. de Groot**, 2010, "Integration of catalysis with storage for the design of multi-electron photochemistry devices for solar fuel," *Appl. Magn. Reson.*, **37**, 497–503.

[20] **H. J. van Gorkom**, 1986, "Photochemistry of photosynthetic reaction centres," *Bioelectrochem. Bioenergetics*, **16**, 77–87.

[21] **D. Noy**, **C. C. Moser**, and **P. L. Dutton**, 2006, "Design and engineering of photosynthetic light-harvesting and electron transfer using length, time, and energy scales," *Biochim. Biophys. Acta*, **1757**(2), 90–105.

[22] **M. Janssen**, **J. Tramper**, **L. R. Mur**, and **R. H. Wijffels**, 2003, "Enclosed outdoor photobioreactors: light regime, photosynthetic efficiency, scale-up, and future prospects," *Biotechnol. Bioeng.*, **81**(2), 193–210.

https://doi.org/10.1017/CBO9780511718786.032 Published online by Cambridge University Press

[23] **S. Bahatyrova**, **R. N. Frese**, **C. A. Siebert** *et al.*, 2004, "The native architecture of a photosynthetic membrane," *Nature*, **430**(7003), 1058–1062.
[24] **J. A. Shelnutt**, **X.-Z. Song**, **J.-G. Ma** *et al.*, 2010, "Nonplanar porphyrins and their significance in proteins," *Chem. Soc. Rev.*, doi:10.1002/chin.199818321.
[25] **A. Pandit**, **F. Buda**, **A. J. van Gammeren**, **S. Ganapathy**, and **H. J. M. De Groot**, 2010, "Selective chemical shift assignment of bacteriochlorophyll *a* in uniformly [^{13}C–^{15}N]-labeled light-harvesting 1 complexes by solid-state NMR in ultrahigh magnetic field," *J. Phys. Chem. B*, **114**(18), 6207–6215.
[26] **A. Pandit**, **P. K. Wawrzyniak**, **A. J. van Gammeren**, *et al.*, 2010, "Nuclear magnetic resonance secondary shifts of a light-harvesting 2 complex reveal local backbone perturbations induced by its higher-order interactions," *Biochemistry*, **49**(3), 478–486.
[27] **R. van Grondelle** and **V. I. Novoderezhkin**, 2006, "Energy transfer in photosynthesis: experimental insights and quantitative models," *Phys. Chem. Chem. Phys.*, **8**, 793–807.
[28] **P. K. Wawrzyniak**, **A. Alia**, **R. G. Schaap** *et al.*, 2008, "Protein-induced geometric constraints and charge transfer in bacteriochlorophyll–histidine complexes in LH2," *Phys. Chem. Chem. Phys.*, **10**(46), 6971–6978.
[29] **R. van Grondelle**, **J. P. Dekker**, **T. Gillbro**, and **V. Sundstrom**, 1994, "Energy-transfer and trapping in photosynthesis," *Biochim. Biophys. Acta – Bioenergetics*, **1187**(1), 1–65.
[30] **Z. Liu**, **H. Yan**, **K. Wang** *et al.*, 2004, "Crystal structure of spinach major light-harvesting complex at 2.72 angstrom resolution," *Nature*, **428**(6980), 287–292.
[31] **B. Robert**, **P. Horton**, **A. A. Pascal** and **A. V. Ruban**, 2004, "Insights into the molecular dynamics of plant light-harvesting proteins *in vivo*," *Trends Plant Sci.*, **9** (8), 385–390.
[32] **M. G. Müller**, **P. Lambrev**, **M. Reus** *et al.*, 2010, "Singlet energy dissipation in the photosystem II light-harvesting complex does not involve energy transfer to carotenoids," *ChemPhySchem*, **11**(6), 1289–1296.
[33] **A. V. Ruban**, **R. Berera**, **C. Ilioaia** *et al.*, 2007, "Identification of a mechanism of photoprotective energy dissipation in higher plants," *Nature*, **450**(7169), 575–U22.
[34] **T. K. Ahn**, **T. J. Avenson**, **M. Ballottari**, *et al.*, 2008, "Architecture of a charge-transfer state regulating light harvesting in a plant antenna protein," *Science*, **320** (5877), 794–779.
[35] **T. Förster**, 1965, "Delocalized excitation and excitation transfer," in *Modern Quantum Chemistry*, ed. **O. Sinanoğlu**, New York, Academic Press, pp. 93–137.
[36] **V. I. Prokhorenko**, **D. B. Steensgaard**, and **A. R. Holzwarth**, 2003, "Exciton theory for supramolecular chlorosomal aggregates: 1. Aggregate size dependence of the linear spectra," *Biophys. J.*, **85**(5), 3173–3186.
[37] **J. H. Golbeck**, 2003, "Photosynthetic reaction centers: so little time, so much to do," *Biophysics Textbook Online*, p. 31.
[38] **R. A. Marcus**, 1956, "On the theory of oxidation–reduction reactions involving electron transfer. 1," *J. Chem. Phys.*, **24**(5), 966–978.
[39] **C. C. Moser**, **J. M. Keske**, **K. Warncke**, **R. S. Farid**, and **P. L. Dutton**, 1992, "Nature of biological electron transfer," *Nature*, **355**(6363), 796–802.
[40] **G. L. Closs** and **J. R. Miller**, 1988, "Intramolecular long-distance electron transfer in organic molecules," *Science*, **240**(4851), 440–447.
[41] **S. Y. Reece** and **D. G. Nocera**, 2009, "Proton-coupled electron transfer in biology: results from synergistic studies in natural and model systems," *Ann. Rev. Biochem.*, **78**, 673–699.
[42] **M. Haumann**, **P. Liebisch**, **C. Müller** *et al.*, 2005, "Photosynthetic O_2 formation tracked by time-resolved X-ray experiments," *Science*, **310**(5750), 1019–1021.
[43] **H. Dau** and **I. Zaharieva**, 2009, "Principles, efficiency, and blueprint character of solar-energy conversion in photosynthetic water oxidation," *Acc. Chem. Res.*, **42** (12), 1861–1870.

https://doi.org/10.1017/CBO9780511718786.032 Published online by Cambridge University Press